Developmental Biology 446 (2019) 180–192

Contents lists available at ScienceDirect

Developmental Biology

journal homepage: www.elsevier.com/locate/developmentalbiology

An extended regulatory landscape drives *Tbx18* activity in a variety of prostate-associated cell lineages

Soumya Negi[a,1], Christopher Chase Bolt[b,1], Huimin Zhang[a], Lisa Stubbs[a,*]

[a] Department of Cell and Developmental Biology, University of Illinois, Urbana-Champaign, United States
[b] École Polytechnique Fédérale de Lausanne, SV ISREC UPDUB, 1015 Lausanne, Switzerland

ABSTRACT

The evolutionarily conserved transcription factor, *Tbx18*, is expressed in a dynamic pattern throughout embryonic and early postnatal life and plays crucial roles in the development of multiple organ systems. Previous studies have indicated that this dynamic function is controlled by an expansive regulatory structure, extending far upstream and downstream of the gene. With the goal of identifying elements that interact with the *Tbx18* promoter in developing prostate, we coupled chromatin conformation capture (4C) and ATAC-seq from embryonic day 18.5 (E18.5) mouse urogenital sinus (UGS), where *Tbx18* is highly expressed. The data revealed dozens of active chromatin elements distributed throughout a 1.5 million base pair topologically associating domain (TAD). To identify cell types contributing to this chromatin signal, we used lineage tracing methods with a *Tbx18 Cre* "knock-in" allele; these data show clearly that *Tbx18*-expressing precursors differentiate into wide array of cell types in multiple tissue compartments, most of which have not been previously reported. We also used a 209 kb *Cre*-expressing *Tbx18* transgene, to partition enhancers for specific precursor types into two rough spatial domains. Within this central 209 kb compartment, we identified ECR1, previously described to regulate *Tbx18* expression in ureter, as an active regulator of UGS expression. Together these data define the diverse fates of *Tbx18+* precursors in prostate-associated tissues for the first time, and identify a highly active TAD controlling the gene's essential function in this tissue.

1. Introduction

The *Tbx18* gene encodes a deeply conserved T-box transcription factor (TF) that is expressed dynamically throughout development, with central roles in the differentiation of mesoderm-derived cell types in a wide variety of embryonic tissues (Naiche et al., 2005; Papaioannou, 2014). As a testament to this gene's essential functions, *Tbx18* null mutant (*Tbx18*$^{-/-}$) mice die perinatally, with abnormalities of the axial skeleton, hydroureter and hydronephrosis as the most obvious visible phenotypes (Airik et al., 2006; Bussen et al., 2004). However, mutant animals also display defects in the heart, kidneys, and inner ear, trabecular bone and other tissues (Bohnenpoll et al., 2013; Cai et al., 2008; Wu et al., 2013).

We previously described a mouse reciprocal translocation, called 12Gso, which breaks approximately 70 kb downstream of the *Tbx18* gene and reduces its function in a tissue- and developmental time-specific manner, creating a hypomorphic loss-of-function (LOF) allele (Bolt et al., 2014). The translocation acts by disrupting a conserved "gene desert" region surrounding *Tbx18,* and separating the *Tbx18* promoter from downstream enhancers including an element called ECR1, which drives the continued expression of *Tbx18* expression during later stages of ureter development. These data indicated that the *Tbx18* gene desert houses a complex regulatory landscape extending far from the gene's promoter. One previous study showed that a *Tbx18*-containing 209 kb bacterial artificial chromosome (BAC) transgene could recapitulate most, but not all, of the gene's pattern of developmental expression (Wang et al., 2009). However, the full extent and structure of the *Tbx18* regulatory domain has not been elucidated in any tissue.

Unlike *Tbx18* full knockout alleles, 12Gso mutant animals can sometimes survive to adulthood, permitting us to examine *Tbx18* LOF phenotypes in tissues that develop postnatally. Using 12Gso together with a *LoxP*-flanked (floxed) conditional *Tbx18* allele we recently showed that *Tbx18* deficiency is associated with significant abnormalities in urethra-proximal regions of the anterior prostate lobe (Bolt et al., 2016). These abnormalities include the failed development

* Corresponding author.
E-mail addresses: snegi2@illinois.edu (S. Negi), christopher.bolt@epfl.ch (C.C. Bolt), huiminzh@illinois.edu (H. Zhang), ljstubbs@illinois.edu (L. Stubbs).
[1] These authors contributed equally.

http://dx.doi.org/10.1016/j.ydbio.2018.11.023
Received 3 October 2018; Received in revised form 13 November 2018; Accepted 29 November 2018
Available online 27 December 2018
0012-1606/ © 2018 Elsevier Inc. All rights reserved.

of stromal smooth muscle cells and the appearance of inflammatory myofibroblasts, accompanied by a massive disorganization of the adjacent epithelium. We further showed that *Tbx18* is expressed transiently in the caudal urogenital sinus (UGS), the embryonic structure from which the prostate develops, during a brief period peaking at embryonic day 18.5 (E18.5), just before the time of birth. Since 12Gso mutants display the prostate phenotype, we reasoned that enhancers essential to UGS expression during this critical perinatal period would be found downstream of the gene, and beyond the boundaries of the 12Gso translocation (Bolt et al., 2016).

With the goal of mapping long-distance enhancers that interact with the *Tbx18* promoter during prostate development, we carried out circular chromosome conformation capture (4C) and transposase-based mapping of open chromatin domains (ATAC-seq) in chromatin isolated from E18.5 UGS tissue. The data reveal an extended landscape of promoter-contacting regions throughout a 1.5–2 million base pair (Mbp) domain surrounding the *Tbx18* gene; this domain is roughly consistent with a region defined as the primary *Tbx18* topologically associating domain (TAD) (Dixon et al., 2012). We combined these chromatin profiles with *Cre*-Lox-based lineage-tracing studies to assign elements controlling *Tbx18* expression in precursor cells with specific adult fates to subdomains within the TAD. Together, these data point to the locations of long-distance enhancers, including the previously identified element ECR1, that regulate *Tbx18* in a surprisingly large array of precursor cell types at a key stage in urogenital tract development.

2. Materials and methods

2.1. Mice and lineage tracing

B6.Cg-Gt(ROSA)26Sor$^{tm6(CAG-ZsGreen1)Hze/J}$ (ZsG) reporter mice (Madisen et al., 2010), *Tbx18:Cre* (Cai et al., 2008) knock-in allele, B6.Cg-Tg(*Tbx18*-iCre)3Fech/J (*Tbx18*:BAC-i*Cre*) transgenic mice (Wang et al., 2009) and ECR1-Lacz transgenic animals (Bolt et al., 2014) were all maintained by crossing heterozygous *Cre*-expressing animals to C3H/HeJ x C57BL/6J hybrid mice. All animal care and procedures in this study were carried out under strict adherence to the Guide for the Care and Use of Laboratory Animals of the National Institutes of Health. The protocol was approved by IACUC with protocol #15245 at the University of Illinois. The *Cre* lineages were studied by breeding male *Tbx18:Cre/+* heterozygous and *Tbx18:Bac-iCre* animals with ZsG/ZsG homozygous females. For timed pregnancies vaginal plugs were checked in the morning after mating and noon was taken as E0.5. Genomic DNA was prepared from tail snips and used for genotyping by PCR. Primers used for PCR are listed in Supplemental Table 6.

2.2. Lineage tracing and immunohistochemistry

Tissues were dissected at the appropriate age in cold phosphate-buffered saline (PBS) and fixed in 4% paraformaldehyde (PFA) overnight at 4 °C. Tissues were dehydrated and fixed in paraffin wax and then cut into 4–6 μm sections. For lineage tracing the green fluorescence (ZsGreen) was visualized directly. For immunohistochemistry, the sections were incubated overnight at 4 °C with the following antibodies MHC (DSHB, MF20, 1:50), NeuN (Millipore, ABN91, 1:200), Serotonin (Novus, 5HT-H209, 1:100). Following washes, the secondary antibodies Donkey anti mouse IgG 594 (Invitrogen, R37115, 1:200) and Goat anti Chicken IgG 594 (Invitrogen, A-11042, 1:200) were applied as appropriate at room temperature for 1 h. After washes, counterstaining with Hoescht 33342 (Invitrogen, H3570) and coverslipping, the sections were imaged in the Hamamatsu Nanozoomer and Carl Zeiss confocal microscope LSM710.

2.3. LacZ staining

For whole-mount LacZ stains the fresh tissue samples were washed and fixed in ice cold 4% PFA and 5-bromo-4-chloro-3-indolyl-β-d-galactopyranoside (X-Gal; Invitrogen, 15520034) staining was applied as per the protocol outlined in (Loughna and Henderson, 2007). For thin section staining, the lower abdomen was isolated, fixed in 4% PFA and frozen in OCT (Tissue-Tek, 4583) media. 10 μm sections were cut and then X-gal was applied, also as outlined by Loughna and Henderson (2007). Nuclear Fast Red (Vector Laboratories, H-3403) was applied for counterstaining the nuclei.

2.4. Chromatin conformation capture (4C)

Chromatin conformation capture was performed essentially as described in (Gheldof et al., 2012) with these modifications. Each individual biological replicate was produced from five male E18.5 urogenital sinuses dissected from CBA × C57BL/6 F1 embryos. Tissues were disaggregated by treatment with collagenase then fixed with 1% PFA for 10 min at room temperature. Approximately five million cells were used for each replicate. Chromatin was digested with three additions of 400U DpnII (NEB cat# R0543), followed by ligation, and a second digest with 400U HindIII (NEB cat# R0104). Independent chromosomal libraries from biological replicates were amplified with viewpoint primers (Suppl Table 1). The forward and reverse primers map to the genomic interval chr9:87626944-87627578 on Mm9. Samples were sequenced on an Illumina HiSeq. 2500 producing 30 million reads per sample. Mapping and the computational identification of peaks were performed on HTSstation (David et al., 2014; Noordermeer et al., 2011). The 4C-seq reads are quantified and normalized by dividing each fragment score by the mean number of fragment scores that are located within a 1Mbp region upstream and downstream of the viewpoint. These profiles were then corrected by the HTSstation algorithm which adjusts for non-specific interactions as a function of linear distance on the DNA strand. The profiles were then smoothed on a sliding window of eleven restriction fragments. All sequences from this project, including 4C and ATA-seq data (below) have been deposited in the GEO database under accession number GSE123102.

2.5. ATAC-seq

ATAC-seq libraries were produced using a pool of 5 male urogenital sinuses that were treated with collagenase to disaggregate into single-cells. Cells were counted and 50,000 individual cells (96% viability) were treated as described in Buenrostro et al. (2015). We sequenced the ATAC library in HiSeq. 2500 in two batches and obtained 55.4 M and 20.6 M single end reads. We trimmed the reads to remove the Nextera transposase sequences at the ends using Trimmomatic (Bolger et al., 2014). We aligned the reads using Bowtie2 with default parameters (Langmead and Salzberg, 2012) to mm9 with a 51% overall alignment rate. We called peaks using Homer (Heinz et al., 2010) using default parameters and generated wiggle files to view on the UCSC browser (Kent et al., 2002). To identify related human regions, we performed a liftOver of these peaks to hg19 in the UCSC browser platform. We cross-referenced the human liftOver coordinates with coordinates of peaks from the Encode DNase1 Hypersensitive Sites (DHS) track (John et al., 2011; Thurman et al., 2012). Additionally, we used Homer to correlate the mouse ATAC-seq peaks to nearest promoter regions genome-wide, and cross-referenced these peak-associated genes to UGS expression levels using our previously published RNA-seq data set from E18.5 UGS (Bolt et al., 2016).

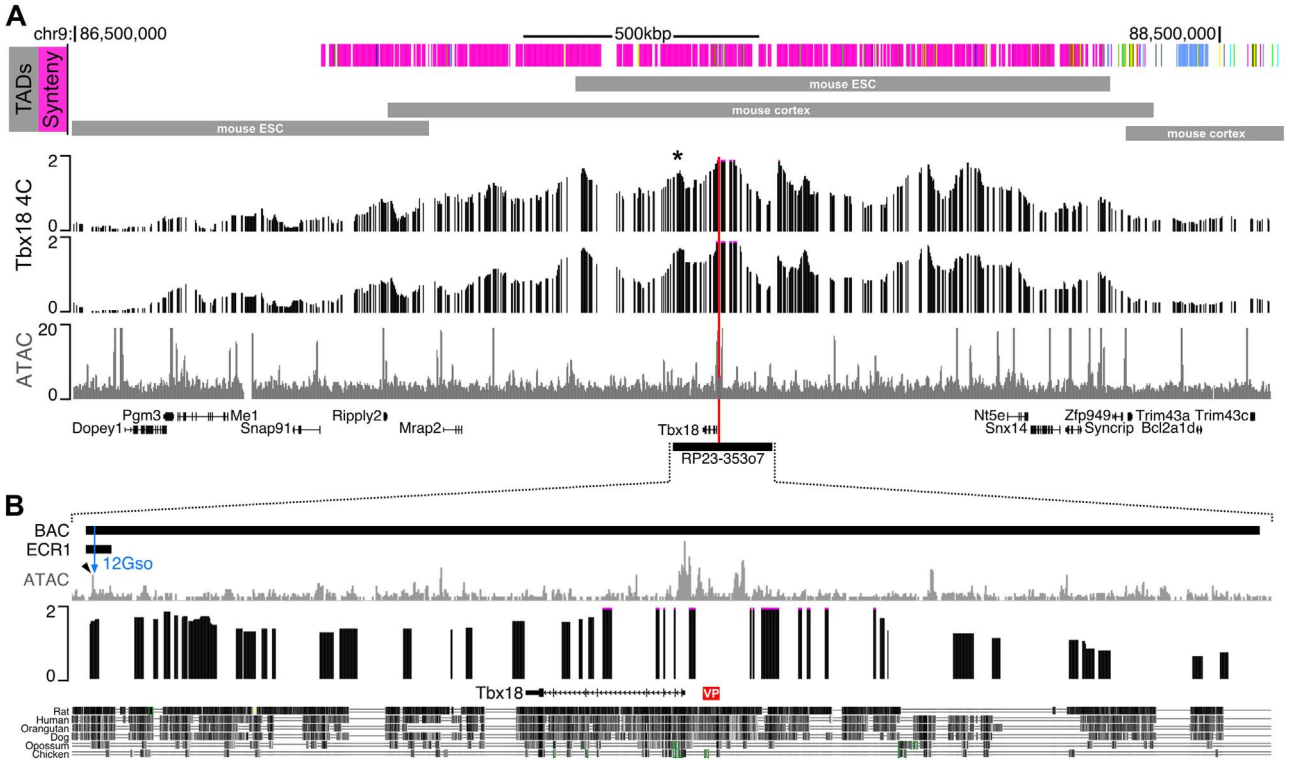

Fig. 1. 4C-seq and ATAC-seq reveal the regulatory structure of the *Tbx18* locus in E18.5 male urogenital sinus. (A) 4C-seq using a viewpoint located at the *Tbx18* promoter (red line) shows the *Tbx18* topologically associating domain extends over a 1.5Mbp region. The asterisk (*) indicates a strong interaction peak with the *Tbx18* promoter. This peak contains the ECR1 enhancer. The indicated TADs are from Dixon et al. (2012) and Lieberman-Aiden et al. (2009)). The two 4C tracks are biological replicates. See Methods section for details on the scaling and smoothing of the 4C. The bottom track of (A) is ATAC-seq for the region. (B) Expansion of the portion of the *Tbx18* locus included in the BAC RP23–353o7. ATAC-seq indicates multiple putative enhancer elements in this subregion. The ECR1 enhancer, which encompasses the 12Gso breakpoint is indicated. This region is also a strong contact for the *Tbx18* promoter and includes a highly accessible element just distal to the 12Gso breakpoint (blue arrowhead). VP is the *Tbx18* 4C-seq viewpoint.

3. Results

3.1. Tbx18 *promoter contacts are distributed throughout a 1.5 Mb topologically associating domain*

To identify regulatory elements contacting the *Tbx18* promoter in the E18.5 male caudal UGS, we carried out circularized chromatin conformation capture (4C) experiments using hight throughput sequencing near the *Tbx18* promoter as the "viewpoint" (see Methods). The experiments were carried out in duplicate on separate pools of tissue and both libraries were sequenced to collect a total of more than 30 million sequence reads. Reads were analyzed using the HTStation software (David et al., 2014) to reveal broad peaks extending from the *Tbx18* promoter both upstream and downstream, over a distance of approximately 2 Mbp (Fig. 1). The highest peak density was found within a smaller region including *Tbx18* neighbors *4922501C03Rik* in the centromeric direction, to *Snx14 and Syncrip* located telomerically (Fig. 1A). This region corresponds roughly to the boundaries of the topologically associating domains (TADs) determined for the *Tbx18* region in mouse and human Hi-C experiments (Fig. 1A) (Dixon et al.).

Synteny is conserved in the human and mouse regions extending 1 Mbp downstream of *Tbx18*, suggesting that the same genes and elements are likely to be in influencing *Tbx18* gene expression in both species. However, an evolutionary rearrangement has disrupted mouse-human synteny upstream of *Tbx18,* in the mouse telomeric direction. Specifically, *Tbx18* and its downstream neighbors, as well as upstream genes up to and including *Syncrip*, are all similarly organized on human chromosome 6 (chr6). However, genes beyond *Syncrip* in mouse chr9 do not map to human chr6; instead they cluster together on human chr4. This evolutionary breakpoint coincides well with the telomeric ends of the experimentally determined, conserved mouse *Tbx18* TAD (Fig. 1A). The TAD contains approximately 10 broad peaks identifying the approximate locations of sequence elements in contact with the *Tbx18* promoter in E18.5 UGS cells, detected with excellent reproducibility in the replicate experiments (Figs. 1 and 4C tracks).

3.2. *Genome-wide open chromatin maps define positions for regulatory elements within* Tbx18 *promoter-contacting peaks*

To more precisely delineate the locations of active enhancers within the broad 4C peaks, we carried out ATAC-seq, a transposase-based method that allows identification of open, or accessible chromatin positions genome-wide from small numbers of input cells (Buenrostro et al., 2015) (Supplemental Table 2).

Open chromatin profiles have not been published for UGS at any developmental stage, making quality genome-wide profiles potentially useful beyond the purposes of this study. To assess the quality of these data, we first asked whether the ATAC-seq peaks correlated well with genome features known to be associated with open chromatin marks in eukaryotic genomes (Suppl Table 2). For example, as expected, E18.5 UGS ATAC-seq peaks were especially enriched near (within 2 kb of) the annotated promoters of genes expressed in the UGS genome-wide; furthermore, most of the peaks with the highest levels of ATAC-seq enrichment were promoter-linked, as expected (Supplemental Table 4). Furthermore, ATAC-seq promoter peak height correlated roughly with previously determined E18.5 UGS gene expression levels ((Bolt et al., 2016), Supplemental Table 3). Thus, the ATAC-seq peaks correlate well with features expected of open chromatin domains.

In addition, a large number of less highly enriched non-promoter peaks were also detected throughout the genome, including in the *Tbx18* TAD region (Supplemental Table 2; Figs. 1A, 1B). All but eight of the ATAC peaks in the *Tbx18* TAD region are well conserved in the human genome, and overlap very well with ENCODE-analyzed DNase1 hyper-sensitive sites determined in a panel of human cell lines

(citation; Suppl. Table 5), suggesting conserved regulatory activity. One of these conserved ATAC-seq peaks with a DNase1 HS site, located under a distal 4C-peak positioned downstream of *Tbx18,* is contained within the previously defined ECR1 enhancer region, which lies near the end of *Tbx18*-containing BAC clone RP23–353o7 (Fig. 1B, Supplemental Table 5).

3.3. Lineage tracing experiments define broad functional territories within the Tbx18 TAD

These data defined a large active TAD with broad 4C peaks containing a significant number of potentially novel UGS enhancers. However, the UGS and closely apposed tissues (which would have been included in our dissections) is comprised of a mix of different cell types at E18.5. ATAC-seq and 4C-seq peaks could be contributed by any relatively abundant UGS cell type. At this developmental stage, undifferentiated mesenchymal cells comprise the predominant cell type, although epithelial cells, neurons, and other cell types are also present in the tissue samples. Enhancers can exist in various regulatory states: active, primed, and poised (Cruz-Molina et al., 2017; Rada-Iglesias et al., 2011; Zentner et al., 2011). In agreement, the observed 4C peaks could represent cells in which *Tbx18* is being actively expressed, repressed, or consisting of a constitutive architectural state at the E18.5 time-point.

To define the cell types expressing *Tbx18* at or around E18.5 with an eye toward later tracing the adult fates of those cells, we used a *Cre-Lox* based lineage-tracing approach. For this purpose, we used a previously published mouse strain in which the *Cre* gene had been "knocked in" to exon 2 of the native *Tbx18* locus (*Tbx18:Cre*; (Cai et al., 2008)). We crossed this strain to animals carrying a ZsGreen (modified GFP) reporter gene held silent by a *loxP*-flanked upstream stop codon (Gt(ROSA)26Sor$^{tm6(CAG-ZsGreen1)Hze}$/J; (Madisen et al., 2010); hereafter abbreviated ZsG). In animals carrying both the *Tbx18:Cre* and ZsG allele, *Tbx18*-expressing (*Tbx18*+) cells will be fluorescently labeled; once the floxed stop codon has been excised by *Cre* in a *Tbx18*+ precursor cell, all descendants of that cell will also be labeled, allowing a determination of their ultimate adult fates.

We also employed lineage mapping for another purpose: that is, with the goal of subdividing the large *Tbx18* TAD into subdomains harboring enhancers active in different subsets of UGS-associated cells. Specifically, we used the 209 kb BAC transgene, described above (*Tbx18*:BAC-*icre*), in which BAC RP23–353o9 has been modified by "knocking in" a *Cre* recombinase gene into the *Tbx18* gene resident in the BAC, and used to create a transgenic mouse line (Wang et al., 2009). As also mentioned, *Tbx18:*BAC-*iCre* drives reporter expression in a pattern that mirrors *Tbx18* expression faithfully in many cell types and tissues, but does not recapitulate all native *Tbx18* domains ((Wang et al., 2009) and see below). This finding is consistent with the fact that the BAC encompasses only a subset of *Tbx18* promoter-contacting DNA elements (Fig. 1B).

Using the *Tbx18:Cre* and *Tbx18*:BAC-*iCre* alleles in parallel thus offered the possibility of subdividing the *Tbx18* TAD into functional subdomains. To test this strategy, we crossed animals carrying each allele to mice carrying the floxed ZsG reporter and collected tissues from doubly heterozygous offspring at different ages. We focused on reporter expression at E18.5, but also collected tissues at later stages with an eye toward identifying the adult fates of the *Tbx18*+ cells. We examined cell types contained within the UGS proper but also closely adherent cells that would have been included in gene expression and chromatin analysis.

We previously reported that the *Tbx18* transcript and protein are expressed in the UGS as early as E16.5 (Bolt et al., 2016). At this stage expression is limited to a cluster of UGS mesenchymal cells that closely surround dorsal and anterior portions of the prostatic urethra (Bolt et al., 2016). The *Tbx18*:BAC-*iCre* allele was also shown previously to drive low level expression from a floxed beta-galactosidase-expressing *LacZ* reporter gene in the UGS as early as E15.5 (Wang et al., 2009). We examined ZsG expression driven both the *Tbx18:Cre* and *Tbx18*:*Bac-iCre* alleles at E16.5, and confirmed low levels of labeling concentrated in the dorsal and anterior regions of the prostatic urethra, very similar to the pattern reported previously (Bolt et al., 2016).

Also consistent with quantitative RT-PCR (qRT-PCR) and immunohistochemistry (IHC) data indicating peak *Tbx18* UGS expression around the time of birth (Bolt et al., 2016), we also detected high levels of ZsG labeling in UGS sections from animals carrying the native *Tbx18:Cre* knock-in together with the floxed ZsG allele (*Tbx18:cre/+*, ZsG/+) at E18.5. We first examined transverse sections taken from a relatively anterior position, near the base of the bladder where the prostate buds have begun to form. At this stage and in this location, *Tbx18:Cre*-driven ZsG labeling was widespread throughout the UGS mesenchyme in both dorsal and ventral directions, including cells surrounding the base of the seminal vesicles (SV) and ejaculatory ducts (ED), around the prostatic urethra (UR), and around the buds of prostatic epithelium extending into the mesenchyme (arrowhead in Fig. 2**A**). In contrast, the *Tbx18*:BAC-*iCre* allele drove ZsG expression primarily in the dorsal portions of the UGS in comparable anterior sections, with limited ventral labeling (Fig. 2**B**).

In more posterior sections of *Tbx18:Cre/+*, ZsG/+ UGS, ZsG expression was driven in cells forming a ring surrounding the urethra (Fig. 2E). However, this domain of ZsG expression was not detected in the *Tbx18*:BAC-*iCre*, ZsG+ embryos (Fig. 2F). The ring of cells labeled by *Tbx18:Cre* yielded a strong positive signal when the sections were stained with an antibody to myosin heavy chain, a marker for skeletal muscle, confirming that the ring of cells labeled exclusively in *Tbx18:Cre/+*, ZsG/+ embryos are skeletal muscle precursors (yellow cells in Fig. 2E). The ring of MHC+ cells was arranged similarly to those that will later give rise to the skeletal muscle of the rhabdosphincter (Borirakchanyavat et al., 1997; Oelrich, 1980; Sebe et al., 2005) (Fig. 6C), suggesting that *Tbx18* is expressed in cells destined for the rhabdosphincter fate.

Also labeled by the endogenous *Tbx18:Cre* knock-in but not by the T*bx18:*BAC-*iCre* allele was the loose band of mesenchymal cells exterior to but in close apposition to the UGS (Figs. 2G, 2I); both *Cre* alleles labeled the mesothelial lining around the developing organ (Fig. 2H. 2J). Although the identification of *Tbx18* expression in skeletal muscle cells was surprising, each of these cell types is mesenchymally derived. Even more surprisingly, however, we found clear examples of ZsG labeling driven from both of the *Cre* alleles in cells of other embryonic types. For example, the *Tbx18:Cre* drove expression of the floxed ZsG reporter in urothelial cells forming the inner lining the prostatic urethra (Fig. 2C); these cells were not labeled by the *Tbx18*:BAC-*iCre* (Fig. 2D). Moreover, with both *Cre* alleles, we saw ZsG expression in the pelvic ganglia (PG), which develop to provide the major innervation of the bladder and prostate (Keast, 2006). Like other peripheral ganglia, PG cells are of neural crest origin (Wiese et al., 2017, 2012) an embryonic lineage not previously linked to *Tbx18* activity. Widespread ZsG labeling was detected in PG with the *Tbx18:Cre* at E18.5, with stronger expression driven by the transgenic *Tbx18*:BAC-*iCre* allele but in a more limited number of PG cells (Figs. 2A, 2B; Figs. 3A, 3D).

The ZsG+ cells in the PG were of two types at this stage in both animals: (1) round cells with large nuclei and cell bodies, and (2) elongated cells, many of which appeared to encase the large round cells (Figs. 2A, 2B; Figs. 3A, 3D). In the PG, these different cell shapes are associated with (1) progenitor cells or differentiated neurons and (2) satellite glia, which wrap and protect sympathetic neurons either singly or in clusters, respectively (Armati and Mathey, 2013). The majority of ZsG+ cells were of the latter type, although especially in the *Tbx18*:BAC-*iCre* images, rounds cells were also brightly labeled with ZsG (Figs. 3A, 3D). We asked whether these round cells were neurons or undifferentiated progenitors by staining sections with NeuN, an established marker for differentiated neuronal cells. In both cases, a

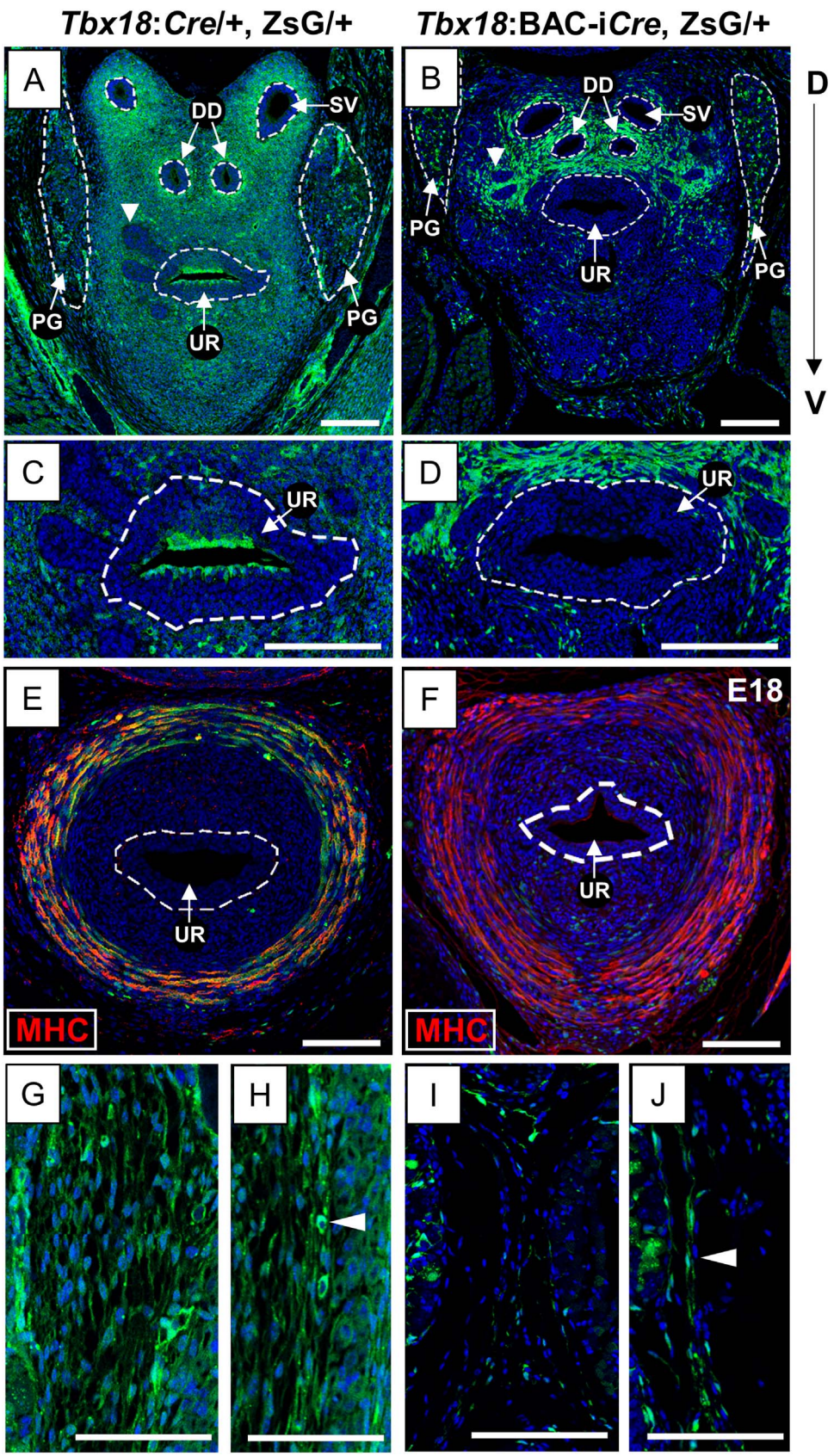

Fig. 2. E18.5 UGS lineage tracing using *Tbx18:Cre* and *Tbx18*:BAC-i*Cre* alleles. Immunofluorescence (A-D, G-J) and Immunohistochemistry (E, F) of transverse sections at E18.5. *Cre*-expressing lineages are marked by ZsGreen (ZsG; Green) and nuclei are counter-stained with Hoechst (Blue). The *Tbx18:Cre* allele gives rise to strong and widespread ZsG labeling in the anterior UGS mesenchyme (A) in contrast to *Tbx18:*BAC-*iCre* which labels cells only in regions dorsal to the UR (B). White arrowheads mark anterior buds (A, B). Surface urethral epithelial cells are labeled by the *Tbx18:Cre* (C) but not by *Tbx18:*BAC-*iCre* allele (D). *Tbx18:Cre* lineage labeling is intense in a ring of posteriorly located muscle cells that becomes the rhabdosphincter (E) but *Tbx18:*BAC-*iCre* does not label these cells (F), which stain positive for the Myosin heavy chain antibody (MHC; in red). The loose mesenchyme surrounding the UGS is labeled with *Tbx18:Cre* (G) but not *Tbx18:*BAC-*iCre* (I); see Figs. 6A, 6B. Mesothelium, marked by white arrowheads (H, J) is marked by both *Cre* alleles. Abbreviations DD: Ductus deferens; PG: Pelvic ganglia; SV: Seminal vesicles; UR: urethra. Scale bars are 100 μm.

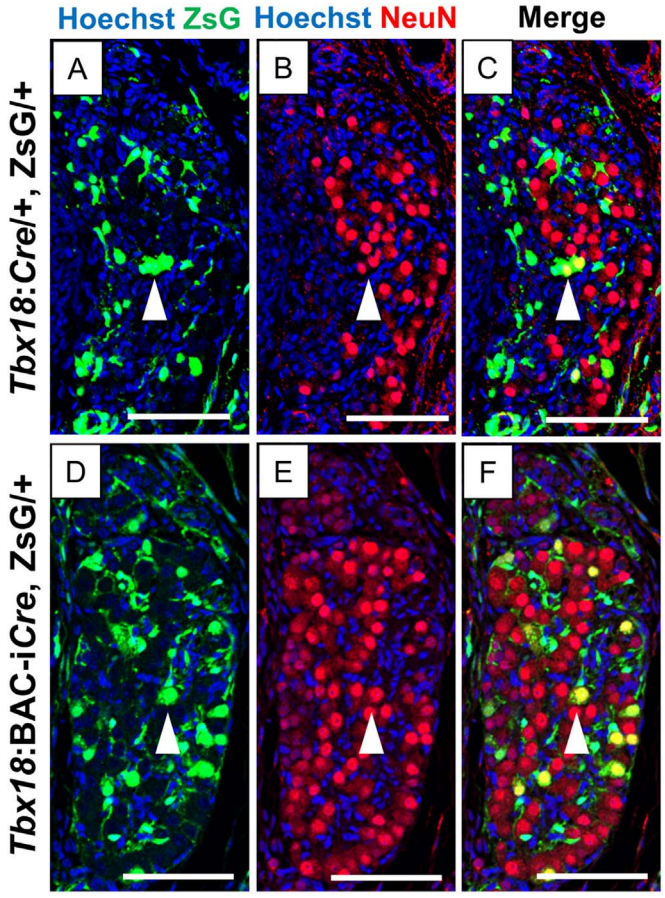

Fig. 3. Cells marked by *Tbx18:Cre* and *Tbx18:*BAC-*iCre* alleles in the E18.5 Pelvic Ganglia. Immunohistochemistry of transverse sections of the pelvic ganglia at E18.5 with the NeuN antibody identify the presence of differentiated neurons. Lineages labeled with the endogenous *Tbx18:Cre* and the *Tbx18:*BAC-*iCre* alleles are marked by ZsGreen (Green) and nuclei are counter-stained with Hoechst (Blue). The *Tbx18:Cre* allele marks a larger population of cells in the pelvic ganglia including a few that co-stain lightly with the neuronal marker NeuN (white arrowheads in A, B, and C). *Tbx18:*BAC-*iCre* also labels cells in the E18.5 pelvic ganglia, and including some brightly stained NeuN+ neurons, arrowheads in (D, E, F). Scale bars are 100 μm.

subset of the NeuN+ cells were also labeled with ZsG, more in number in the *Tbx18*:BAC-*iCre* sections than for the *Tbx18:Cre* samples (arrowheads in Figs. 3C, 3F). In sections from animals of both genotypes, the elongated glial cells were labeled with ZsG but did not co-stain with NeuN, as expected. However, in both cases, we detected NeuN+ cells without ZsG label. These data suggested that the *Tbx18:Cre* and *Tbx18*:BAC-*iCre* drive expression in progenitor cells somewhere along the path to the commitment to neuron or glial cell lineages, with the fate of labeled cells biased toward the satellite glial cell fate.

3.4. *Adult fates of* Tbx18-*expressing UGS cells*

To better understand the identities of labeled cell types, and in particular the ultimate fates of those cells, we also examined prostates and closely associated supporting tissues from adult animals. Both *Cre* alleles labeled cells in the fibromuscular stroma of the prostate lobes, particularly in urethral-proximal regions of the anterior and dorsolateral lobes (Fig. 4**A-F**). In animals carrying either *Cre* allele, ZsG-labeled cells corresponded to both major prostate stromal cell types, fibroblasts and SMC, as evidenced by staining with vimentin (VIM), and smooth muscle actin (SMA) antibodies, respectively (Fig. 4G-J). We also detected bright ZsG labeling in other cell types in and around the prostate lobes including some with a surprising connection to *Tbx18*.

For example, in the prostate epithelial compartment we detected isolated, dispersed cells in both genotypes; staining with the serotonin (5-HT) antibody revealed all of these to be the neuroendocrine cells (NEC) of the prostate (Fig. 5E-F, arrowheads). Like cells within the PG, NEC are derived from neural crest precursors (Szczyrba et al., 2017), making this a second type of *Tbx18+* cells of this lineage. Within the adult pelvic ganglia, most ZsG+ cells were of the satellite glial type, stretched around neuronal cells in a continuous, elongated layer (Fig. 5C,), stained with s100, a marker for satellite glia (Yan and Keast, 2008). These elongated cells were also labeled with ZsG+ in the *Tbx18*:BAC-*iCre* animals (Fig. 5D); additionally, and uniquely in the *Tbx18*:BAC-*iCre*, ZsG+ mice, the cell bodies of large, round cells were labeled (Fig. 5Bi). These round cell bodies also tested positive for NeuN (Fig. 5Bii) indicating that, *Tbx18*:BAC-*iCre* actively drives *Cre* expression in precursors of both pelvic ganglion satellite glia and neuronal cells. We also saw lineages of both *Tbx18:Cre* and *Tbx18:*BAC-*iCre* in cells around blood vessels (data not shown).

Looking at other cell types closely associated with the prostate but not integral to it, we detected very strong ZsG labeling in the adult adipose tissue with the *Tbx18:Cre* allele (Fig. 6A). ZsG was also detected within the same periprostatic adipose depots in *Tbx18*:BAC-*iCre,* ZsG+ mice, but in significantly fewer cells and at much reduced intensity (Fig. 6B). This difference suggests that mesenchymal cells destined to differentiate into prostate-associated adipocytes express *Cre* from the native *Tbx18* allele, but not, or significantly less so, from the *Tbx18*:BAC-*iCre* transgene. The exact origins of these fat depots is not clear, but they should be derived from a mesenchymal cell type not labeled with the *Tbx18:*BAC-*iCre* allele. Candidate tissues thus include the loose band of mesenchymal cells surrounding the UGS at E18.5 (Fig. 2G), or possibly, cells of the anterior/ventral regions of the E18.5 UGS. Alternatively, the periprostatic fat cells could be derived from cells outside the UGS proper, or from cells that express *Tbx18* after E18.5. Whatever their origins, these data show that *Tbx18* is expressed in cells that are fated to become periprostatic fat.

A final stark difference between the two *Cre*-expressing alleles was observed in the very strong labeling of skeletal muscle cells of the external rhabdosphincter in mice driving ZsG from *Tbx18:Cre* (Fig. 6C); these muscle cells were not labeled in animals expressing ZsG from the *Tbx18*:BAC-*iCre* driver (Fig. 6D). This result is consistent with activities of the two *Cre* alleles in the ventrally- and caudally-located ring of mesenchymal cells at E18.5 (Figs. 2E, 2F), and confirms the *Tbx18+* origins of those skeletal muscle cells.

3.5. *The ECR1 enhancer is expressed in developing prostate*

Together these data define cell types expressing *Tbx18* in the E18.5 UGS, including a majority of mesenchymal cells with a surprising variety of adult cell fates, but also a less numerous but nonetheless significant population of cells derived from the neural crest. The comparison between expression driven by *Tbx18:Cre* and the *Tbx18*:BAC-*iCre* transgene allow us to divide the *Tbx18* TAD region into rough functional domains, including enhancers within the boundaries of the BAC transgene or beyond its limits, either upstream or downstream of the *Tbx18* gene (Fig. 8). Thus, we can surmise that elements functional in the population of UGS mesenchymal cells that give rise to most prostate-associated adipose tissue and skeletal muscle in the external rhabdosphincter, map outside the region spanned by BAC RP23–353o7. On the other hand, enhancers required for expression of *Tbx18* in stromal fibroblasts and SMC, neuroendocrine cells within the prostate epithelial compartment, and satellite glia within the pelvic ganglia appear to all be contained within the 209 kb BAC region (Fig. 8).

Previously, we leveraged the fact that the 12Gso translocation breaks just within the region spanned by BAC RP23–353o7 to identify the ECR1 enhancer, which is required to maintain expression of *Tbx18* in later embryonic stages of ureter development (Bolt et al., 2014).

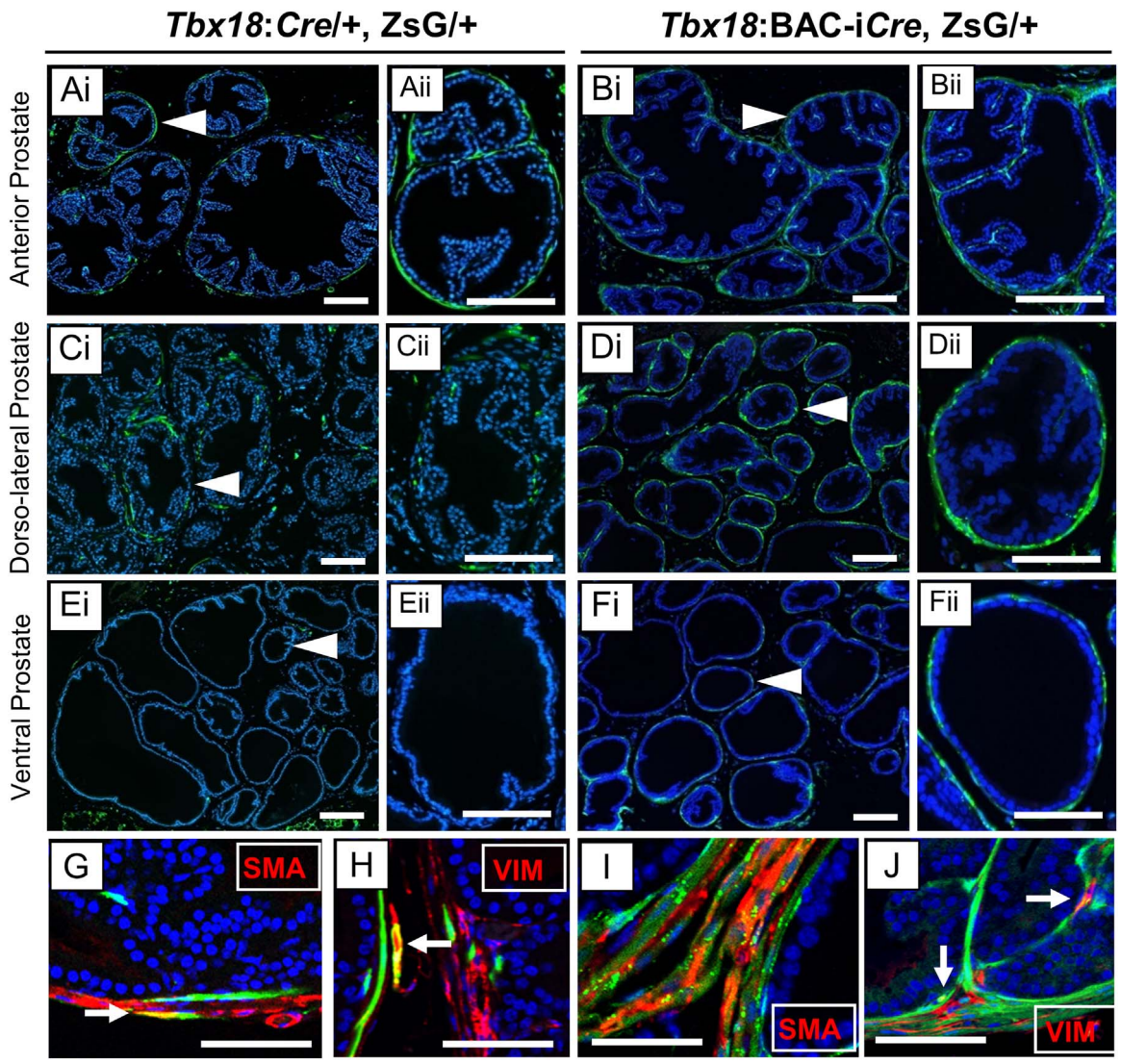

Fig. 4. Adult lineages labeled by *Tbx18:Cre* and *Tbx18:*BAC-*iCre* alleles in the prostate. *Cre*-expressing lineages are marked by ZsGreen (Green) and nuclei are counter-stained with Hoechst (Blue). Panels marked by roman numeral ii (Aii-Fii) are high resolution images crops of areas marked by arrowheads in the corresponding roman numeral i panels (Ai-Fi). *Tbx18:Cre* labels cells the prostatic stroma derived from mesenchymal cells in the Anterior lobe (A), and Dorso-lateral lobe (C) but not in the ventral lobe (E). The *Tbx18:*BAC-*iCre* allele, in contrast, labels stromal cells in all three lobes (B, D,F). Immunohistochemistry of the stroma cells using antibodies that are markers verify the identity of the cell types (G-J). *Tbx18:Cre* and *Tbx18:*BAC-*iCre* label the smooth muscle cells (G, I), marked by smooth muscle actin (SMA), and fibroblasts (H, J), stained with marker Vimentin (VIM). White arrows point to overlap of lineage-traced cells with each marker (G-J). Scale bars correspond to 50 μm.

Interestingly, the ECR1 sequence also includes the only ATAC peak we found within the most distal 4C peak included in the BAC (Fig. 1B). These data suggested that ECR1 is active in developing UGS as well as in the ureter. The enhancer marked by the E18.5 UGS ATAC-seq peak is at the centromeric end of ECR1, and thus located just beyond the 12Gso breakpoint site (Fig. 1B). Along with any other enhancers downstream of the translocation breakpoint, separation of this ECR1-encompassed enhancer from the *Tbx18* promoter could thus play a functional role in the prostate phenotype we detected in *Tbx18* mutant mice (Bolt et al., 2016).

We showed previously that ECR1 drives expression in developing ureteric mesenchyme by analyzing expression of a transgenic construct containing this sequence element, cloned upstream of a *LacZ*-expressing enhancer reporter (Bolt et al., 2014). To ask whether ECR1 is expressed in developing prostate, we collected UGS from the same transgenic line and stained the sectioned tissue with the colorimetric reporter X-gal.

The data confirmed that ECR1 indeed can drive reporter expression in the E18.5 UGS. Enhancer activity is highest in the mesenchymal cells clustered closely adjacent to and dorsal of the prostatic urethra, in a pattern very similar to the *Tbx18* expression pattern at E16.5 (Fig. 7C). Transverse sections collected from anterior to posterior positions (rostrally-to-caudally) throughout the E18.5 UGS of ECR1 transgenic mice provided a three-dimensional view of the enhancer's activity. Mesenchymal cells scattered around the UGS mesenchyme and just beginning to condense around the distal tips some prostatic buds were also labeled by the ECR1-driven reporter, although at much less intense levels than the urethra-proximal cells at this developmental stage (Fig. 7E). These *LacZ*-expressing mesenchymal cells represent a subset of the expression pattern driven by the *Tbx18*-BAC-*iCre* allele at this same time point (Fig. 2B, refer to ZsG staining), consistent with the fact that ECR1 sequence is contained within the region spanned by BAC RP23–353o7. In addition, a small number of cells were labeled in the E18.5 pelvic ganglia; in this case, the cells labeled by ECR1

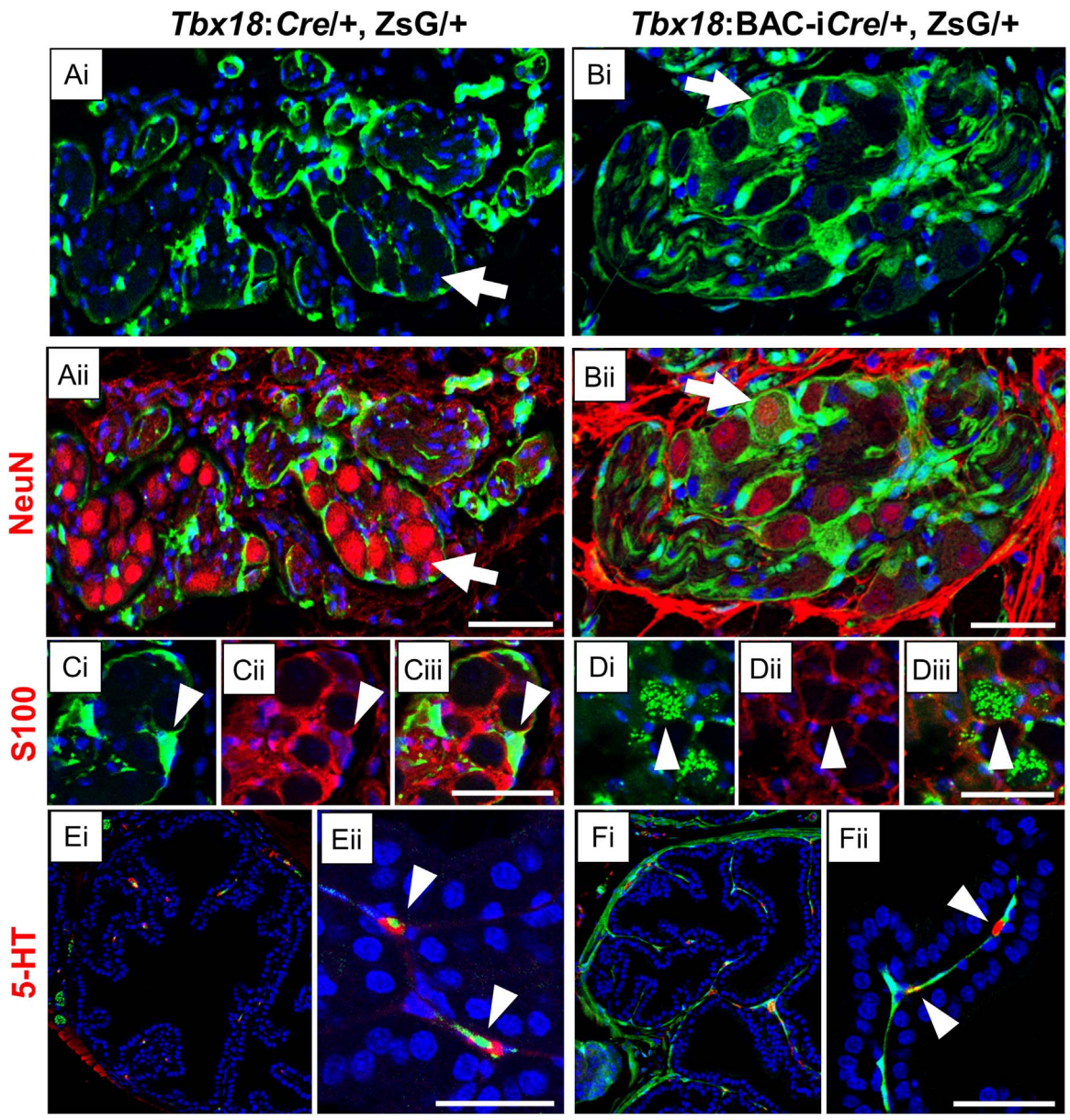

Fig. 5. *Tbx18:Cre* and *Tbx18:*BAC-*iCre* expressing cells give rise to adult neurons and glia. *Cre*-expressing lineages are marked by ZsGreen (Green) and nuclei are counter-stained with Hoechst (Blue). *Tbx18:Cre* and *Tbx18:*BAC-*iCre* strongly label lineages in the pelvic ganglia (A-D) as well as neuroendocrine cells (E, F) in the prostate epithelial compartment. Panels A-D include sub-panels marked with roman numerals that are the same section imaged with different wavelength channels. *Tbx18:Cre* does not label mature neurons in the pelvic ganglia, which are stained with the neuronal NeuN antibody (Aii), although these mature neurons are labeled by the *Tbx18:*BAC-*iCre* (Bii); white arrows. All cells marked in the pelvic ganglia by the *Tbx18:Cre* are satellite glia cells that wrap around the neurons, detected with marker S100 (Ci-iii). *Tbx18:*BAC-*iCre* also labels the satellite glia (Di-iii); white arrowheads. In addition, both *Cre* alleles mark neuroendocrine cells within the prostate epithelial compartment strongly (E-F), as confirmed by staining with an antibody to Serotonin (5-HT). Panels (Eii, Fii) are high resolution images crops of their corresponding panels (Ei, Fi) with arrowheads pointing to neuroendocrine cells. Scale bars correspond to 50 μm.

corresponded to much smaller number than labeled by the BAC transgene (Fig. 3D). These data indicate that promoter-contacting sequences within this downstream 4C peak contain an enhancer driving *Tbx18* expression in urethral-proximal mesenchymal cells in the E18.5 prostate and a subset of pelvic ganglion cells.

4. Discussion and conclusions

Previous studies have pointed to a large and complex regulatory domain for the *Tbx18* gene (Bolt et al., 2014), and the primary purpose of this study was to define the reach, subdomain structure, and cell type-specific regulatory activities within this domain in developing prostate. The data confirm that in E18.5 UGS, the *Tbx18* promoter is in contact with chromatin elements spread over a large domain, corresponding well in both size and position to the regional topologically associating domain determined by Hi-C experiments in human and mouse (Dixon et al., 2012). Within the broad 4C peaks, ATAC-seq peaks highlighted smaller regions of accessible chromatin, suggesting more precisely the positions of potential active enhancer elements active in the UGS at E18.5. Since most of these accessible elements in the *Tbx18* region are conserved and correspond to DNase1 hypersensitive sites in human cells, homologous sequences are likely to correspond to enhancers driving *Tbx18* expression during human prostate development as well. To our knowledge, this is the first report of accessible chromatin elements in the UGS at any developmental time point or in any species, and these data thus provide a resource with potential utility beyond the specific aims of this work.

Our original expectation was that *Tbx18*-expressing UGS cells would correspond primarily to mesenchymal cells destined to develop into stromal smooth muscle cells and fibroblasts of the anterior and

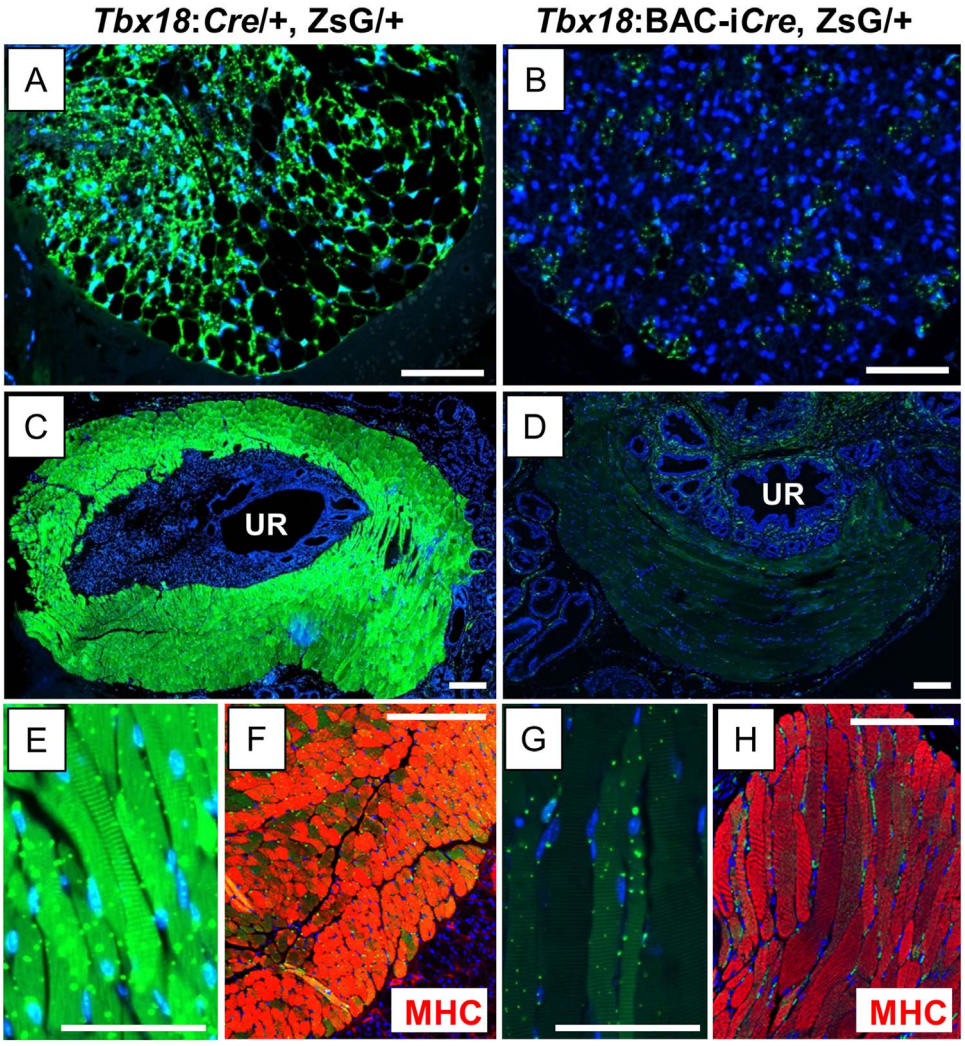

Fig. 6. *Tbx18:Cre* and *Tbx18:*BAC-*iCre* differentially mark adult periprostatic adipose cells and skeletal muscle of the rhabdosphincter. *Cre*-expressing lineages are marked by ZsGreen (Green) and nuclei are counter-stained with Hoechst (Blue). Periprostatic fat and rhabdosphincter are each marked strongly by *Tbx18:Cre* (A, C) but not by *Tbx18:*BAC-*iCre* (B, D) respectively. E, G are high magnification crops of C, D showing striations in the muscle. The striated *Tbx18:Cre*-labeled rhabdosphincter cells stain very strongly with the Myosin heavy chain antibody, a marker for striated muscle (F) but these cells are not labeled with *Tbx18:*BAC-*iCre*. Scale bars correspond to 100 μm.

dorsolateral prostate lobes – which, we have shown, are grossly abnormal in *Tbx18* mutant adults (Bolt et al., 2016). We therefore expected the chromatin data we generated to represent that particular class of mesenchymal precursor cells. Mesenchymal precursors do indeed represent the primary *Tbx18*+ UGS cell type at this stage, although lineage studies have revealed that these precursor cells adopt a surprisingly wide variety of adult cellular fates. Most of the adult cell types labeled strongly by *Tbx18:Cre* in adults - stromal smooth muscle cells, fibroblasts, and periprostatic adipose – develop postnatally, and their precursors remain undifferentiated at E18.5 (Georgas et al., 2015). The *Tbx18*+ cells at this stage might therefore reasonably be expected to present relatively consistent gene expression and chromatin profiles.

Nevertheless, several lines of evidence suggest that the *Tbx*18+ UGS mesenchymal precursors are not identical, even at this early stage. For example, as illustrated by ECR1, specific enhancers may be active only in spatially restricted subsets of these cells. Even more strikingly, mesenchymal cells forming the ventral and posterior ring around the urethral have already begun to express the myosin heavy chain protein by E18.5 and to display signs of striation, indicating that these cells are already committed to the skeletal muscle fate. These rhabdosphincter precursors are relatively numerous, and are thus likely to contribute unique chromatin and gene expression patterns to the composite tissue signals.

The very strong labeling of rhabdosphincter cells was a major surprise to arise from our lineage tracing studies, because *Tbx18* has not been reported to be expressed in skeletal muscle precursors in the past. However, compared to other skeletal muscle types, rhabdosphincter cells have an unusual origin and differentiation history. Specifically, these cells are derived from splanchnic rather than from somatic mesenchyme, reportedly sharing a common embryonic precursor with smooth muscle cells of the lissopshincter (Sebe et al., 2005). Rhabdosphincter skeletal muscle cells have been reported to transdifferentiate from smooth muscle, a highly unusual origin for skeletal muscle cells (Borirakchanyavat et al., 1997). Rhabdosphincter is central to stress urinary continence and thus of significant medical importance (Koraitim, 2008), and the developmental trajectory of these cells remains uncertain (Georgas et al., 2015). The identification of *Tbx18* as a transcription factor that is active in the precursors of rhabdosphincter cells may thus provide a useful tool for future studies as well as be used as a good lineage marker for this muscle.

Even more surprisingly, we identified *Tbx*18+ cells that are of embryonic lineages not previously associated with *Tbx18*. These

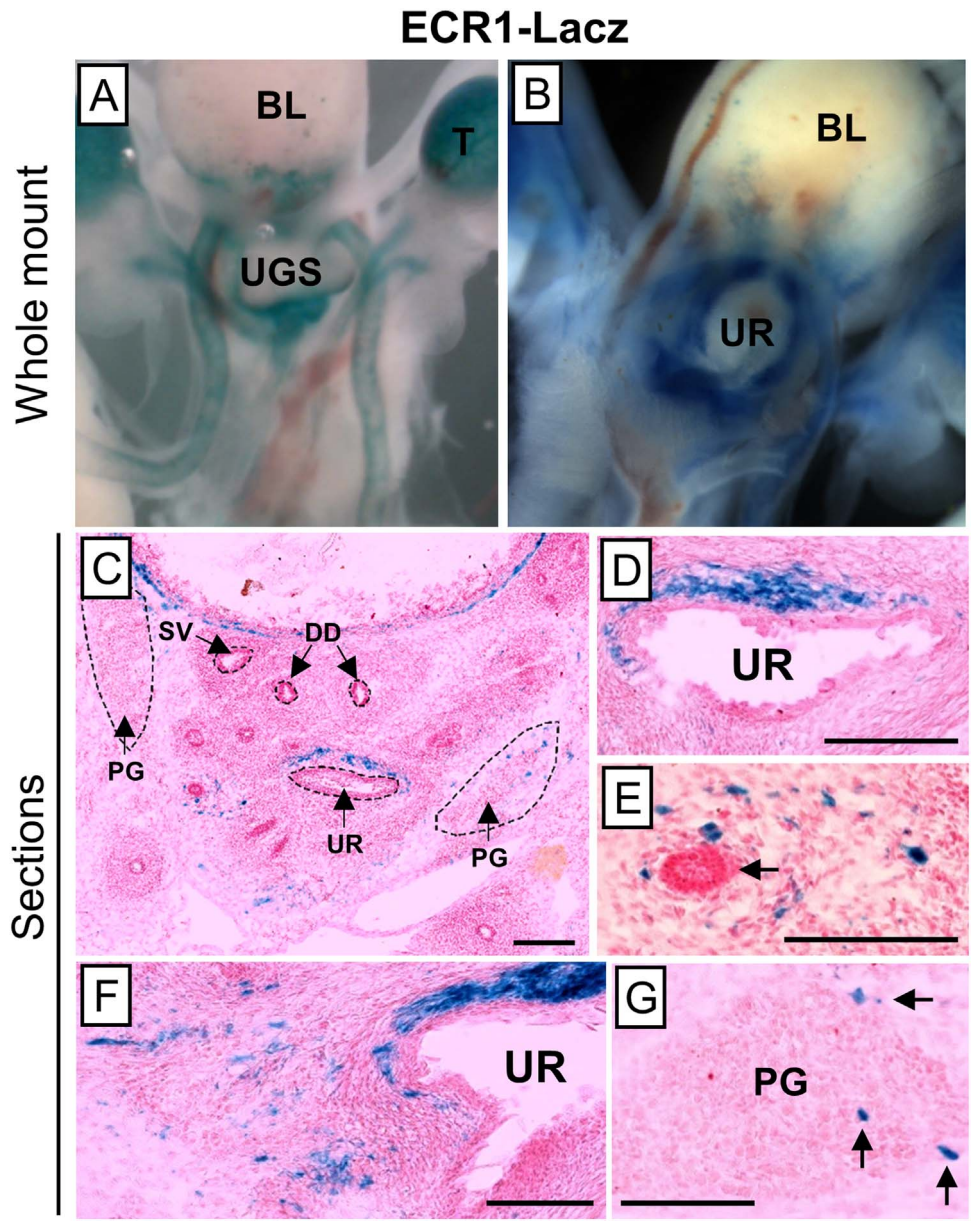

Fig. 7. ECR1 expression in the E18.5 UGS. Using the Ecr1-Lacz transgenic animals we examined expression of the enhancer in thet E18.5 UGS using βgal staining. Whole-mount sections showed strong expression in the UGS (A, B). To identify cell types and regions expressing LacZ, βgal staining was done on 10 μm sections (C-G). ECR1 expression is highest in the mesenchyme located just dorsal to the prostatic urethra (C, D, E). Mesenchymal expression is also detected around the prostatic buds (E, F; black arrow in E points to a dorso-lateral bud). ECR1 expression is further seen in a small number of cells the pelvic ganglia (G). Scale bars are 100 μm.

include a limited number of cells of endodermal origin, which form the inner epithelial lining of the embryonic prostatic urethra; we detected no labeling of urethral epithelium or known derivative cells in adults, suggesting either that this *Tbx*18+ population is transient, or that they adopt adult fates that are currently undocumented. A second, more numerous group of cells expressing *Tbx18* at E18.5 are known to be derived from the neural crest; these include particularly the precursors of satellite glia in the pelvic ganglia but also the neuroendocrine cells that are sparsely distributed throughout the adult epithelial compartment. The cells giving rise to satellite glia are weakly labeled by the *Tbx18:Cre* at E16.5 (data not shown), but are very strongly labeled by E18.5, indicating active *Tbx18* expression at or just before this later developmental stage. The origins of neuroendocrine cells and when *Tbx18* might be expressed in those cells was not captured in this study. This is the first report of *Tbx18* expression in neural crest-derived cells in any tissue, and suggest further investigation of the T-Box protein's role in their differentiation and function. Glial progenitor cells are particularly interesting in the context of this study, since they are present in sufficient numbers to contribute to significant signals in both chromatin and expression data discussed here.

With two *Tbx18 Cre* alleles used for lineage-tracing studies, we were also able to partition the *Tbx18* TAD into regional subdomains housing regulatory elements expressed in specific subpopulations of cells. In particular, expression of *Cre* from the endogenous *Tbx18* allele marks the full range of cell types summarized above. *Cre* driven by the *Tbx18:*BAC-*iCre* transgene, representing genomic material that surrounds *Tbx18* by 209 kb, also labels many of these cell types suggesting that active enhancers required for *Tbx18* expression in these cells are present within the BAC. However, rhabdosphincter precursors or most cells giving rise to periprostatic fat are not labeled by the *Tbx18:*BAC-*Cre* transgene, suggesting that enhancers required for *Tbx18* expression in precursors to those cell types lie outside the 209 kb BAC region (Fig. 8).

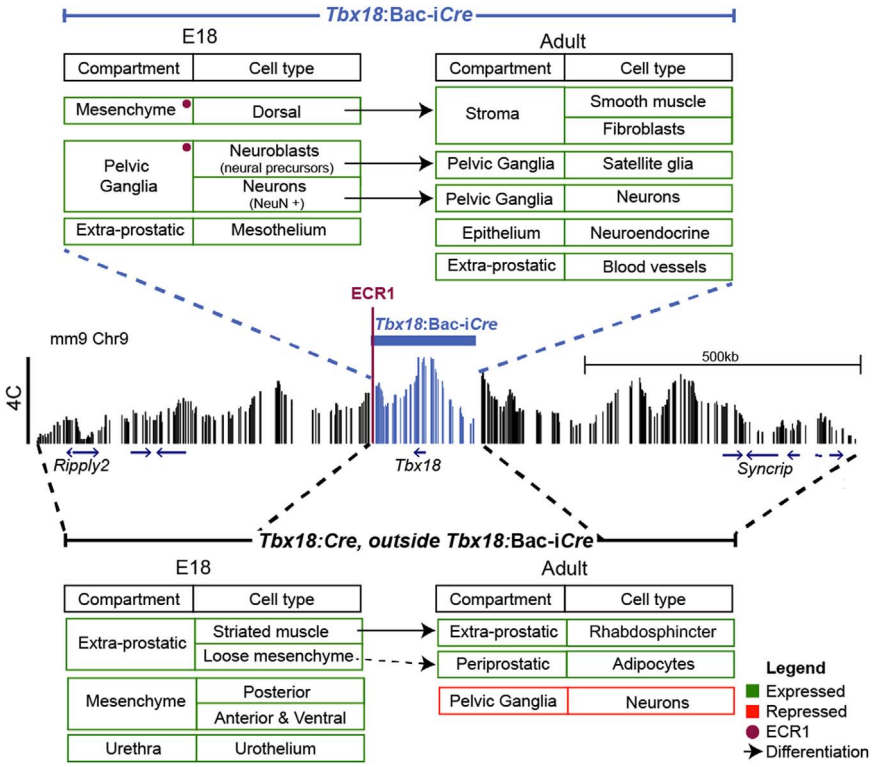

Fig. 8. Regulatory map of the *Tbx18* locus divided into 2 broad regions. Comparison of the cell lineages of the two Cres at E18.5 and in adults gives us the lineages controlled by the regulatory elements contained inside the 209 kb BAC. The *Tbx18*-Bac-i*Cre* region captures most of the cell fates, except the striated muscle, loose mesenchyme, ventral mesenchyme and the urothelium at E18.5. This suggests that the enhancer for these cell fates lie outside the BAC, but within the 1.5 Mb TAD. In addition we hypothesize that as *Tbx18:Cre* lacks lineages in Neurons there is a repressive element contained outside the BAC region. The 4.5kbp regulatory element ECR1 close to the end of the BAC is expressed by a subset of the cells expresses by the BAC marked with the red dot.

Another distinction between the *Tbx18:Cre* and *Tbx18:*BAC-*iCre* alleles concerns the fates assumed by labeled cells in the pelvic ganglia in adult. In particular, the *Tbx18:*BAC-*iCre* allele appears to strongly label differentiated neurons, while the endogenous *Tbx18:Cre* does not. While other explanations are possible, we hypothesize that this difference may suggest the presence of a repressor element located outside the region spanned by the BAC, which serves to silence *Tbx18* expression in common neuron-glia precursors after their commitment to the neuronal fate. The other explanation of this difference could be that the *Tbx18*:BAC-i*Cre* is turned on earlier in the neuron-glia precursor lineage due to the absence of a repressive element outside the BAC region than the native *Tbx18:Cre* allele, and so marks both the neurons and glial cells. Future experiments will aim to test these hypotheses.

In addition to lending information regarding regulatory domain structure, lineage tracing studies reveal novel information that further inform the role of *Tbx18* in urogenital development and health. In particular, we had interpreted the prostate phenotype in *Tbx18* mutants as resulting from a failure of the *Tbx*18+ precursors of stromal smooth muscle cells and fibroblasts to differentiate appropriately (Bolt et al., 2016). These stromal cells are clearly malformed in the mutant mice, and their developmental failure could explain epithelial abnormalities through the disruption of essential mesenchymal:epithelial signaling (reviewed by Cunha (2008)) and through inflammatory signals generated by the myofibroblasts that appear instead of differentiated smooth muscle cells (Tuxhorn et al., 2002).

However, *Tbx18+* precursors give rise to a much wider range of cell types, including several known to strongly impact prostate epithelial development, growth and maintenance in adults, and these must now be taken into account. For example, *Tbx18+* cells of mesenchymal origin directed to blood vessels and periprostatic fat depots could each contribute significantly to prostate epithelial health (Hayakawa and Wang, 2017; Laurent et al., 2016; Zahalka et al., 2017). Furthermore, satellite glia are essential to the survival and function of pelvic ganglion neurons (reviewed by Armati and Mathey (2013),) and dysfunction of these neurons has in turn been associated with prostate disorders (Hayakawa and Wang, 2017; McVary et al., 1994; Thiyagarajan, 2002; Wang et al., 1991; Zahalka et al., 2017). Neuroendocrine cells are also essential to the health of the prostate epithelium, providing neuropeptide hormones with profound effects on epithelial function and growth (Abrahamsson and di Sant'Agnese, 1993; Gkonos et al., 1995). These data suggest many paths through which *Tbx18* dysfunction might directly affect the development growth or maintenance of prostate epithelia throughout the lifespan. Fortunately, these paths can be examined individually through conditional knockouts and appropriate *Cre* alleles.

Lineage tracing studies also revealed potential roles for *Tbx18* that may be highly relevant to urogenital health. Specifically, the very high and uniform expression of *Tbx18* in mesenchymal cells giving rise to the rhabdosphincter, a tissue that is independently critical to urogenital health, suggest that *Tbx18* could be involved in development of other types of important lower urogenital tract disorders.

Finally, we show that an enhancer driving *Tbx18* expression in the developing ureter (Bolt et al., 2014) is also active during early stages of prostate development. ECR1 is active in a subset of the dorsal mesenchymal cells that are labeled with the *Tbx18*:BAC-*iCre,* consisting primarily of a tight band of cells cluster just dorsal and adjacent to the prostatic urethra. This expression subset makes sense, since ECR1 is wholly contained within the boundaries of the BAC transgene (Bolt et al., 2014). In fact, the ECR1 expression pattern resembles the earliest pattern of expression we detected with a TBX18 antibody, which is also tightly clustered in this dorsal position at E16.5. We thus conjecture that ECR1 may be expressed in this domain before the E18.5 timepoint, remaining active in this location through later stages

when the *Tbx18* expression domain increases to include a wider swath of UGS mesenchymal cells. Previously we had shown a conserved *Lef1* binding site in ECR1 (Bolt et al., 2014) and other studies in the ureter have suggested a role of canonical WNT signaling in maintaining expression of *Tbx18* in the condensing mesenchyme around ureteric buds (Airik et al., 2006; Trowe et al., 2012). This data along with our observation of ECR1 expression at E18.5 resembling the early pattern of expression of *Tbx18* (detected with antibody staining at E16.5), suggests that WNT signaling maintains *Tbx18* expression at E18.5 around the condensing prostatic buds through activation of ECR1.

The ATAC-seq peaks underlying the major 4C contact points suggest locations of additional enhancers that interact with the *Tbx18* promoter and drive expression in additional mesenchymal and neural crest-derived domains. Future studies will be focused on exploiting this resource for a deeper look at the surprising range of developmental functions involving *Tbx18*.

Acknowledgments

We are very grateful to Dr. Feng Chen, University of Washington, St Louis for very generously contributing the *Tbx18:BAC-iCre* animal, and Dr. Sylvia Evans, University of California San Diego, for providing the *Tbx18:Cre*. We also thank Seeon Lee, Jennifer Yoo, and Kurt Reynolds, for expert assistance with mouse breeding, genotyping and histological analysis. We also thank Dr. Denis Duboule, EPFL, for contributing intellectual resources and time. This work was supported by Grant number DK095685 from the U.S. National Institute of Diabetes and Digestive and Kidney Disorders (awarded to L.S.). C.C.B is supported by the National Institute of Child Health and Human Development NRSA (F32HD093555).

Author contributions

Conceived and designed the experiments: SN CCB LS. Performed the experiments: SN CCB HZ. Analyzed the data: SN CCB LS. Wrote the paper: SN CCB LS.

Appendix A. Supplementary material

Supplementary data associated with this article can be found in the online version at doi:10.1016/j.ydbio.2018.11.023.

References

Abrahamsson, P.A., di Sant'Agnese, P.A., 1993. Neuroendocrine cells in the human prostate gland. J. Androl. 14, 307–309.
Airik, R., Bussen, M., Singh, M.K., Petry, M., Kispert, A., 2006. Tbx18 regulates the development of the ureteral mesenchyme. J. Clin. Investig. 116, 663–674.
Armati, P.J., Mathey, E.K., 2013. An update on Schwann cell biology–immunomodulation, neural regulation and other surprises. J. Neurol. Sci. 333, 68–72.
Bohnenpoll, T., Bettenhausen, E., Weiss, A.C., Foik, A.B., Trowe, M.O., Blank, P., Airik, R., Kispert, A., 2013. Tbx18 expression demarcates multipotent precursor populations in the developing urogenital system but is exclusively required within the ureteric mesenchymal lineage to suppress a renal stromal fate. Dev. Biol. 380, 25–36.
Bolger, A.M., Lohse, M., Usadel, B., 2014. Trimmomatic: a flexible trimmer for Illumina sequence data. Bioinformatics 30, 2114–2120.
Bolt, C.C., Elso, C.M., Lu, X., Pan, F., Kispert, A., Stubbs, L., 2014. A distant downstream enhancer directs essential expression of Tbx18 in urogenital tissues. Dev. Biol. 392, 483–493.
Bolt, C.C., Negi, S., Guimarães-Camboa, N., Zhang, H., Troy, J.M., Lu, X., Kispert, A., Evans, S.M., Stubbs, L., 2016. Tbx18 regulates the differentiation of periductal smooth muscle stroma and the maintenance of epithelial integrity in the prostate. PLoS One 11, e0154413.
Borirakchanyavat, S., Aboseif, S.R., Carroll, P.R., Tanagho, E.A., Lue, T.F., 1997. Continence mechanism of the isolated female urethra: an anatomical study of the intrapelvic somatic nerves. J. Urol. 158, 822–826.
Buenrostro, J.D., Wu, B., Chang, H.Y., Greenleaf, W.J., 2015. ATAC-seq: a method for assaying chromatin accessibility genome-wide. Curr. Protoc. Mol. Biol. 109, (21.29.21-29).
Bussen, M., Petry, M., Schuster-Gossler, K., Leitges, M., Gossler, A., Kispert, A., 2004. The T-box transcription factor Tbx18 maintains the separation of anterior and posterior somite compartments. Genes Dev. 18, 1209–1221.
Cai, C.L., Martin, J.C., Sun, Y., Cui, L., Wang, L., Ouyang, K., Yang, L., Bu, L., Liang, X., Zhang, X., Stallcup, W.B., Denton, C.P., McCulloch, A., Chen, J., Evans, S.M., 2008. A myocardial lineage derives from Tbx18 epicardial cells. Nature 454, 104–108.
Cruz-Molina, S., Respuela, P., Tebartz, C., Kolovos, P., Nikolic, M., Fueyo, R., van Ijcken, W.F.J., Grosveld, F., Frommolt, P., Bazzi, H., Rada-Iglesias, A., 2017. PRC2 facilitates the regulatory topology required for poised enhancer function during pluripotent stem cell differentiation. Cell Stem Cell 20, 689–705, (e689).
Cunha, G.R., 2008. Mesenchymal-epithelial interactions: past, present, and future. Differ. Res. Biol. Divers. 76, 578–586.
David, F.P., Delafontaine, J., Carat, S., Ross, F.J., Lefebvre, G., Jarosz, Y., Sinclair, L., Noordermeer, D., Rougemont, J., Leleu, M., 2014. HTSstation: a web application and open-access libraries for high-throughput sequencing data analysis. PLoS One 9, e85879.
Dixon, J.R., Selvaraj, S., Yue, F., Kim, A., Li, Y., Shen, Y., Hu, M., Liu, J.S., Ren, B., 2012. Topological domains in mammalian genomes identified by analysis of chromatin interactions. Nature 485, 376–380.
Georgas, K.M., Armstrong, J., Keast, J.R., Larkins, C.E., McHugh, K.M., Southard-Smith, E.M., Cohn, M.J., Batourina, E., Dan, H., Schneider, K., Buehler, D.P., Wiese, C.B., Brennan, J., Davies, J.A., Harding, S.D., Baldock, R.A., Little, M.H., Vezina, C.M., Mendelsohn, C., 2015. An illustrated anatomical ontology of the developing mouse lower urogenital tract. Development 142, 1893–1908.
Gheldof, N., Leleu, M., Noordermeer, D., Rougemont, J., Reymond, A., 2012. Detecting long-range chromatin interactions using the chromosome conformation capture sequencing (4C-seq) method. Methods Mol. Biol. 786, 211–225.
Gkonos, P.J., Krongrad, A., Roos, B.A., 1995. Neuroendocrine peptides in the prostate. Urol. Res. 23, 81–87.
Hayakawa, Y., Wang, T.C., 2017. Nerves switch on angiogenic metabolism. Science 358, 305–306.
Heinz, S., Benner, C., Spann, N., Bertolino, E., Lin, Y.C., Laslo, P., Cheng, J.X., Murre, C., Singh, H., Glass, C.K., 2010. Simple combinations of lineage-determining transcription factors prime cis-regulatory elements required for macrophage and B cell identities. Mol. Cell 38, 576–589.
John, S., Sabo, P.J., Thurman, R.E., Sung, M.H., Biddie, S.C., Johnson, T.A., Hager, G.L., Stamatoyannopoulos, J.A., 2011. Chromatin accessibility pre-determines glucocorticoid receptor binding patterns. Nat. Genet. 43, 264–268.
Keast, J.R., 2006. Plasticity of pelvic autonomic ganglia and urogenital innervation. Int. Rev. Cytol. 248, 141–208.
Kent, W.J., Sugnet, C.W., Furey, T.S., Roskin, K.M., Pringle, T.H., Zahler, A.M., Haussler, D., 2002. The human genome browser at UCSC. Genome Res. 12, 996–1006.
Koraitim, M.M., 2008. The male urethral sphincter complex revisited: an anatomical concept and its physiological correlate. J. Urol. 179, 1683–1689.
Langmead, B., Salzberg, S.L., 2012. Fast gapped-read alignment with Bowtie 2. Nat. Methods 9, 357–359.
Laurent, V., Guerard, A., Mazerolles, C., Le Gonidec, S., Toulet, A., Nieto, L., Zaidi, F., Majed, B., Garandeau, D., Socrier, Y., Golzio, M., Cadoudal, T., Chaoui, K., Dray, C., Monsarrat, B., Schiltz, O., Wang, Y.Y., Couderc, B., Valet, P., Malavaud, B., Muller, C., 2016. Periprostatic adipocytes act as a driving force for prostate cancer progression in obesity. Nat. Commun. 7, 10230.
Lieberman-Aiden, E., van Berkum, N.L., Williams, L., Imakaev, M., Ragoczy, T., Telling, A., Amit, I., Lajoie, B.R., Sabo, P.J., Dorschner, M.O., Sandstrom, R., Bernstein, B., Bender, M.A., Groudine, M., Gnirke, A., Stamatoyannopoulos, J., Mirny, L.A., Lander, E.S., Dekker, J., 2009. Comprehensive mapping of long-range interactions reveals folding principles of the human genome. Science 326, 289–293.
Loughna, S., Henderson, D., 2007. Methodologies for staining and visualisation of beta-galactosidase in mouse embryos and tissues. Methods Mol. Biol. 411, 1–11.
Madisen, L., Zwingman, T.A., Sunkin, S.M., Oh, S.W., Zariwala, H.A., Gu, H., Ng, L.L., Palmiter, R.D., Hawrylycz, M.J., Jones, A.R., Lein, E.S., Zeng, H., 2010. A robust and high-throughput Cre reporting and characterization system for the whole mouse brain. Nat. Neurosci. 13, 133–140.
McVary, K.T., Razzaq, A., Lee, C., Venegas, M.F., Rademaker, A., McKenna, K.E., 1994. Growth of the rat prostate gland is facilitated by the autonomic nervous system. Biol. Reprod. 51, 99–107.
Naiche, L.A., Harrelson, Z., Kelly, R.G., Papaioannou, V.E., 2005. T-box genes in vertebrate development. Annu. Rev. Genet. 39, 219–239.
Noordermeer, D., Leleu, M., Splinter, E., Rougemont, J., De Laat, W., Duboule, D., 2011. The dynamic architecture of Hox gene clusters. Science 334, 222–225.
Oelrich, T.M., 1980. The urethral sphincter muscle in the male. Am. J. Anat. 158, 229–246.
Papaioannou, V.E., 2014. The T-box gene family: emerging roles in development, stem cells and cancer. Development, 3819–3833.
Rada-Iglesias, A., Bajpai, R., Swigut, T., Brugmann, S.A., Flynn, R.A., Wysocka, J., 2011. A unique chromatin signature uncovers early developmental enhancers in humans. Nature 470, 279–283.
Sebe, P., Oswald, J., Fritsch, H., Aigner, F., Bartsch, G., Radmayr, C., 2005. An embryological study of fetal development of the rectourethralis muscle–does it really exist? J. Urol. 173, 583–586.
Szczyrba, J., Niesen, A., Wagner, M., Wandernoth, P.M., Aumuller, G., Wennemuth, G., 2017. Neuroendocrine cells of the prostate derive from the neural crest. J. Biol. Chem. 292, 2021–2031.
Thiyagarajan, M., 2002. alpha-Adrenoceptor antagonists in the treatment of benign prostate hyperplasia. Pharmacology 65, 119–128.
Thurman, R.E., Rynes, E., Humbert, R., Vierstra, J., Maurano, M.T., Haugen, E., Sheffield, N.C., Stergachis, A.B., Wang, H., Vernot, B., Garg, K., John, S., Sandstrom, R., Bates, D., Boatman, L., Canfield, T.K., Diegel, M., Dunn, D., Ebersol, A.K., Frum,

T., Giste, E., Johnson, A.K., Johnson, E.M., Kutyavin, T., Lajoie, B., Lee, B.K., Lee, K., London, D., Lotakis, D., Neph, S., Neri, F., Nguyen, E.D., Qu, H., Reynolds, A.P., Roach, V., Safi, A., Sanchez, M.E., Sanyal, A., Shafer, A., Simon, J.M., Song, L., Vong, S., Weaver, M., Yan, Y., Zhang, Z., Lenhard, B., Tewari, M., Dorschner, M.O., Hansen, R.S., Navas, P.A., Stamatoyannopoulos, G., Iyer, V.R., Lieb, J.D., Sunyaev, S.R., Akey, J.M., Sabo, P.J., Kaul, R., Furey, T.S., Dekker, J., Crawford, G.E., Stamatoyannopoulos, J.A., 2012. The accessible chromatin landscape of the human genome. Nature 489, 75–82.

Trowe, M.O., Airik, R., Weiss, A.C., Farin, H.F., Foik, A.B., Bettenhausen, E., Schuster-Gossler, K., Taketo, M.M., Kispert, A., 2012. Canonical Wnt signaling regulates smooth muscle precursor development in the mouse ureter. Development 139, 3099–3108.

Tuxhorn, J.A., Ayala, G.E., Smith, M.J., Smith, V.C., Dang, T.D., Rowley, D.R., 2002. Reactive stroma in human prostate cancer: induction of myofibroblast phenotype and extracellular matrix remodeling. Clin. Cancer Res.: Off. J. Am. Assoc. Cancer Res. 8, 2912–2923.

Wang, J.M., McKenna, K.E., McVary, K.T., Lee, C., 1991. Requirement of innervation for maintenance of structural and functional integrity in the rat prostate. Biol. Reprod. 44, 1171–1176.

Wang, Y., Tripathi, P., Guo, Q., Coussens, M., Ma, L., Chen, F., 2009. Cre/lox recombination in the lower urinary tract. Genesis 47, 409–413.

Wiese, C.B., Deal, K.K., Ireland, S.J., Cantrell, V.A., Southard-Smith, E.M., 2017. Migration pathways of sacral neural crest during development of lower urogenital tract innervation. Dev. Biol. 429, 356–369.

Wiese, C.B., Ireland, S., Fleming, N.L., Yu, J., Valerius, M.T., Georgas, K., Chiu, H.S., Brennan, J., Armstrong, J., Little, M.H., McMahon, A.P., Southard-Smith, E.M., 2012. A genome-wide screen to identify transcription factors expressed in pelvic Ganglia of the lower urinary tract. Front. Neurosci. 6, 130.

Wu, S.P., Dong, X.R., Regan, J.N., Su, C., Majesky, M.W., 2013. Tbx18 regulates development of the epicardium and coronary vessels. Dev. Biol. 383, 307–320.

Yan, H., Keast, J.R., 2008. Neurturin regulates postnatal differentiation of parasympathetic pelvic ganglion neurons, initial axonal projections, and maintenance of terminal fields in male urogenital organs. J. Comp. Neurol. 507, 1169–1183.

Zahalka, A.H., Arnal-Estape, A., Maryanovich, M., Nakahara, F., Cruz, C.D., Finley, L.W.S., Frenette, P.S., 2017. Adrenergic nerves activate an angio-metabolic switch in prostate cancer. Science 358, 321–326.

Zentner, G.E., Tesar, P.J., Scacheri, P.C., 2011. Epigenetic signatures distinguish multiple classes of enhancers with distinct cellular functions. Genome Res. 21, 1273–1283.